A Numerical Study of Flexural Buckling of Foliated Rock Slopes

D.P. Adhikary[1], H.-B. Mühlhaus[2] and A.V. Dyskin[1]

1. Dept. of Civil Engineering, The University of Western Australia, Australia
2. CSIRO Division of Exploration and Mining, WA, Australia

Abstract: The occurrence of foliated rock masses is common in mining practice. Methods employing continuum approximation in describing the deformation of such rock masses possess a clear advantage over methods where each rock layer and each inter-layer interface (joint) is explicitly modelled. In devising such a continuum model it is imperative that moment (couple) stresses and internal rotations associated with the bending of the rock layers be properly incorporated in the model formulation. Such an approach will lead to a Cosserat-type theory. In the present model, the behaviour of the intact rock layer is assumed to be linearly elastic and the joints are assumed to be elastic perfectly plastic. Condition of slip at the interfaces are determined by a Mohr-Coulomb criterion with tension cut off at zero normal stress. The theory is valid for large deformations. The model is incorporated into the finite element program AFENA and validated against an analytical solution of elementary buckling problems of a layered medium under gravity loading. A design chart suitable for assessing the stability of slopes in foliated rock masses against flexural buckling failure has been developed. The design chart is easy to use and provides a quick estimate of critical loading factors for slopes in foliated rock masses. It is shown that

the model based on Euler's buckling theory as proposed by Cavers [1] substantially overestimates the critical heights for a vertical slope and underestimates the same for sub-vertical slopes.

KEY WORDS: Foliated Rock, Large Deformation, Buckling, Equivalent Continuum

1. Introduction

Often, rock masses are observed to be intersected by a single set of steeply dipping discontinuities, such as regular bedding planes, foliation or joints, producing so called foliated (layered) rock masses. Foliated rock masses are common in mining practices. When a slope is excavated in such a rock mass, besides the normal slip type of failure, two additional modes of failures have to be considered: 1) if the discontinuity plane dips inside the rock mass (Figure 1a), the individual rock layers may bend into the excavation thus giving rise to a class of so called flexural toppling failures; 2) when the discontinuity plane dips more or less parallel to the slope face (Figure 1b), the rock layers may buckle under their own weight giving rise to a so called buckling failure. In figure 1, tentative geometry of the slopes after deformation is sketched by dashed lines. The mechanism of flexural toppling has been discussed in detail in Adhikary et. al [2, 3] and Adhikary and Dyskin [4]. This paper will focus only on the buckling mode of slopes in foliated rock masses.

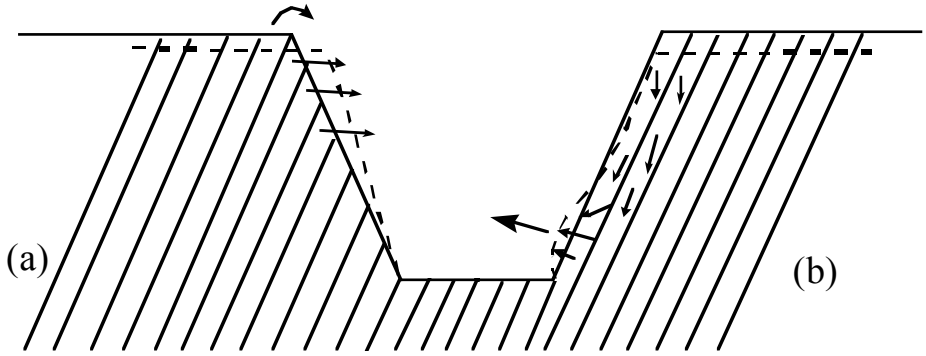

Figure 1. A schematic of slopes in a foliated rock mass:
(a) Flexural toppling and (b) Flexural buckling

Discussions on buckling failures of slopes in sedimentary rocks such as layered coal deposits and sandstones and in schistose metamorphic rocks can be found in [1, 5-9]. Cavers [1] utilizes the concept of Euler's buckling load and derives an expression for critical slope heights. In order to obtain the expression for the critical slope height, Cavers [1] assumes that only a certain portion of the rock layer located in the slope toe region will buckle in reality; the rest of the rock layer simply provides an axial load to the buckling portion of the rock layer. On the basis of base friction model tests, he found out that the ratio of the length of the rock layer actually undergoing buckling (which will be called from now on as effective length) to the total rock layer length ranges in between 0.36-0.46. In his further calculations he assumes this ratio to be equal to 0.5 and obtains the expression for the critical rock layer length. This expression can be rearranged to yield the following expression for a non-dimensional term which we will name as critical loading parameter:

$$\frac{\gamma H^3}{Eh^2} = \frac{\pi^2}{2.25}\left(\sin\alpha - \cos\alpha \tan\phi_j\right)^{-1} \tag{1}$$

where, γ is the unit weight of the rock layer, E is the effective elastic modulus of the rock layer in the direction of layering, H is the slope height, h is the layer thickness

(joint spacing), ϕ_j is the joint friction angle and α is the slope angle (i.e. the layer inclination angle).

The assumption, that a fixed (effective) length of the rock layer undergoes buckling, imposes an unwarranted constraint in model formulation. Indeed, it is more natural to assume that it may well depend on the slope angle and hence any calculation conducted with the fixed layer length ratio may overestimate the critical heights for a vertical slope and underestimate the same for the gentler slopes. Moreover, Cavers [1] only partially incorporates the stabilising effects of the component of forces acting in the direction perpendicular to the rock layer by considering only the shear resistive forces generated along the inter-layer interface (joints). The stabilising effect of the compressive force itself is completely neglected in his formulation. Thus, for a hypothetical slope with smooth inter layer interfaces (ie. zero joint friction angle), the effects of such a compressive force acting in the direction perpendicular to the direction of rock layering will simply vanish in such type of models. In addition, unilateral nature of buckling of foliated slopes is observed to be ignored in previous studies.

The present paper is aimed at presenting a comprehensive numerical model that is valid for large deformations and applying this model for analysing the flexural buckling phenomena in foliated rock masses such that the effective length ratio (i.e. buckling layer length ratio discussed earlier) is no longer considered as an input parameter of the model but it remains a function of the slope geometry and evolves automatically during numerical computation.

This is achieved by formulating a continuum model of layered materials on the basis of the Cosserat theory [10]. The Cosserat theory of elasticity incorporates a local rotation of material points as an independent parameter in addition to the translation assumed in the classical continuum, and couple (moment) stresses (moments per unit area) in addition to the classical (force) stresses (forces per unit area). In Mühlhaus [11] and Zvolinskii and Shkhinek [12], a Cosserat model was formulated for the case of elastic joints. A Cosserat model with elastic-plastic joints was formulated in Adhikary et. al [2], Adhikary and Dyskin [4, 13]. In these earlier models, the deformation is assumed to be infinitesimal and hence their applicability is limited.

The following assumptions are made in the present study: a) the slope is dry; b) the intact layers are perfectly elastic, homogeneous and isotropic, and free from any cross-joint; c) the inter-layer interfaces (joints) are planar and the mechanical properties of each discrete joint are equal; d) the layer thickness (joint spacing) is constant and much smaller than the characteristic length of the external stress variations; e) the plane strain conditions are satisfied; and f) the behaviour of the rock mass is time independent.

2. Cosserat theory

a) Cosserat deformation measures in plane strain

We will first consider infinitesimal deformations and then subsequently propose a simple generalisation for large deformation. A local rigid cross is assigned to every material point (x_1, x_2) of the body in a Cartesian coordinate system (X_1, X_2). The layering is assumed to be parallel to the X_1-direction. In the process of deformation,

the material points (rigid crosses) may undergo rotations by an angle $__3$ about the X_3-axis in addition to the translations given by the displacements (u_1, u_2).

For the formulation of constitutive relationships, we need deformation measures which are invariant with respect to rigid body motions. In the conventional, infinitesimal continuum theory, this requirement leads to the strain tensor,

$$\varepsilon_{ij} = \tfrac{1}{2}\left(u_{i,j} + u_{j,i}\right) \quad u_{i,j} = \frac{\partial u_i}{\partial x_j}, \quad i,j = 1,2 \tag{2}$$

In the Cosserat theory, we have two other invariant deformation measures, namely

$$\Omega_3^{rel} = \omega_3 - \Omega_3, \qquad \omega_3 = \tfrac{1}{2}\left(u_{2,1} - u_{1,2}\right) \tag{3}$$

which represents the relative rotation between the material element and the corresponding rigid coordinate cross, and

$$\kappa_{3i} = \Omega_{3,i} \tag{4}$$

which is a measure for the relative rotation between neighbouring rigid crosses. It is usual to combine equations (2) and (3) into a single, tensorial deformation measure (Mühlhaus, 1993), namely:

$$\gamma_{11} = \partial u_1 / \partial x_1, \; \gamma_{21} = \partial u_1 / \partial x_2 + \Omega_3, \; \gamma_{22} = \partial u_2 / \partial x_2, \; \gamma_{12} = \partial u_2 / \partial x_1 - \Omega_3 \tag{5}$$

Then,

$$\varepsilon_{ij} = \tfrac{1}{2}\left(\gamma_{ij} + \gamma_{ji}\right) \qquad \Omega_3^{rel} = \tfrac{1}{2}\left(\gamma_{12} - \gamma_{21}\right) \tag{6}$$

For the treatment of large deformation problems, we require an appropriate generalisation of the relative deformation tensor γ_{ij} and the curvature tensor κ_{3i} (here, i, j = 1, 2). Perhaps the most straight-forward generalisation of γ_{ij} [14]:

$$\Gamma = \left(\boldsymbol{R}^{c}\right)^{T} \boldsymbol{F} \tag{7}$$

where, $\boldsymbol{F}$ is the deformation gradient and $\boldsymbol{R}^{c}$ is the rotation tensor of the Cosserat rigid cross. When the Cosserat rotation is equal to the rotation $\boldsymbol{R}$ of an infinitesimal element of the continuum, then it follows from the polar decomposition $\boldsymbol{F}=\boldsymbol{R}\boldsymbol{U}$ such that $\Gamma = \boldsymbol{U}$, where $\boldsymbol{U}$ is the right Cauchy-Green tensor [14]. For infinitesimal deformation $\Gamma_{ij} - \delta_{ij}$ reduces to γ_{ij} .

The starting point for the derivation of large deformation theory is the virtual work principle. This paper deals with only a relatively simple variant of the general theory similar to that assumed in the engineering beam and plate buckling theories in which the geometric non-linearity associated with the curvatures and couple stresses is neglected. In the incremental form of the virtual work expression, this can be expressed as [14]:

$$\Delta\delta W = \int_{b} \Delta\sigma_{ij}\delta\gamma_{ij} dV + \int_{b} \sigma_{ij}\Delta\delta\Gamma_{ij} dV + \int_{b} \Delta m_{3k}\delta\kappa_{3k} dV \tag{8}$$

where

$$\Delta\delta\mathfrak{I}_{ij} = \delta\mathfrak{Q}_{ki}\Delta\gamma_{kj} + \Delta\mathfrak{Q}_{ki}\delta u_{k,j} \quad \text{and} \quad \mathfrak{Q}_{ki} = -e_{ki3}\mathfrak{Q}_{3} \tag{9}$$

Here, e_{ki3} is the permutation symbol, b denotes the domain of integration in the undeformed configuration. Terms of third and higher order have been dropped. It should be mentioned that in the present formulation σ_{ij} does not designate the Cauchy stress tensor, but rather the energy conjugate to $\mathfrak{I}_{ij}$.

From the principle of virtual work, a simple calculation yields the following system of equations:

$$t_{ij,j} = 0 \quad \text{and} \quad e_{ij3}\left(\Delta\tau_{ij} - \sigma_{jk}\Delta\gamma_{ik}\right) = 0 \tag{10}$$

where,

$$t_{ij} = \Delta\tau_{ij} + \sigma_{kj}\Delta\Omega_{ik} \quad \text{and} \quad \Delta\tau_{ij} = \Delta\sigma_{ij} - \Delta m_{3i,i} \tag{11}$$

By an expansion of (10) with the use of (11), the local moment and angular moment balance are obtained as:

$$\Delta\sigma_{11,1} - \left(\sigma_{12}\Delta\Omega_3\right)_{,1} + \Delta\sigma_{21,2} - \left(\sigma_{22}\Delta\Omega_3\right)_{,2} = 0 \tag{12}$$

$$\Delta\sigma_{22,2} + \left(\sigma_{21,2}\Delta\Omega_3\right)_{,2} + \Delta\sigma_{12,1} + \left(\sigma_{11}\Delta\Omega_3\right)_{,1} = 0 \tag{13}$$

$$\Delta\sigma_{21} - \Delta\sigma_{12} - \Delta m_{31,1} - \sigma_{12}\Delta\gamma_{11} + \sigma_{11}\Delta\gamma_{12} - \sigma_{22}\Delta\gamma_{21} + \sigma_{21}\Delta\gamma_{22} = 0 \tag{14}$$

It is worthwhile to mention that the last four terms in Eq. (14) do not have any noticeable influence on the computed results in the application considered in this study.

b) Constitutive relationships

The layer interfaces can exhibit three different modes of behaviour: (a) elastically connected with the interface normal and shear stiffness (k_n and k_s), (b) disconnected with frictional sliding and (c) disconnected with tensile opening. This kind of behaviour is best described by relations of elasto-plastic type. With this in mind, the rate of the deformation vector are decomposed into an elastic and a plastic part (see Eq. 18 and 19 for the definition of pseudo vectors), *viz*

$$\dot{\vec{e}} = \dot{\vec{e}}_e + \dot{\vec{e}}_p \tag{15}$$

For the criterion of interface sliding, f_s, and the corresponding plastic potential, g_s, we assume:

$$f_s = \left|\sigma_{21}\right| + tg\phi_j \sigma_{22} - c_j \le 0, \quad g_s = \left|\sigma_{21}\right| \tag{16}$$

where ϕ_j and c_j designate the angle of friction and the cohesion of the joints respectively. Similarly, the criterion for the tensile opening and the corresponding plastic potential are written as:

$$f_t = \sigma_{22} \; ? \; 0, \quad g_t = \sigma_{22} \tag{17}$$

For the explicit representation of the stress-strain relationship in terms of tensor components, it is advantageous to introduce pseudo-vector and matrix notation as follows:

$$\vec{\sigma} = \left\{\sigma_{11}, \sigma_{22}, \sigma_{21}, \sigma_{12}, \mu_{31}, \mu_{32}\right\} \tag{18}$$

$$\vec{e} = \left\{\gamma_{11}, \gamma_{22}, \gamma_{21}, \gamma_{12}, \kappa_1, \kappa_2\right\} \tag{19}$$

The superscribed arrows distinguish pseudo-vectors from true vectors and tensors. The elasto-plastic relationships in the general form can be expressed as:

$$\vec{\sigma} = \left[D_{ep}\right]\vec{\dot{e}} \tag{20}$$

where

$$D_{ep} = D_e - \alpha \frac{D_e \; \frac{fg}{f\vec{\sigma}} \; \frac{ff}{f\vec{\sigma}}^{T} \; D_e}{\frac{fg}{f\vec{\sigma}}^{T} \; D_e \; \frac{ff}{f\vec{\sigma}}} \tag{21}$$

Here α is defined as:

$$\alpha = 1 \;\; if \;\; f_s = 0 \;\; and \;\; \dot{\lambda}\,(plastic\ multiplier) > 0; \;\; 0 \;\; if \;\; f_s < 0 \;\; and/or \;\; \dot{\lambda} \le 0 \qquad (22)$$

The course of derivation leading to Eq. (21) is exactly the same as in standard continua so we need not to go into further details here. For the present layered material, the elasticity matrix $\left|D_e\right|$ reads

$$D_e = \begin{matrix} A_{11} & A_{12} & 0 & 0 & 0 & 0 \\ & A_{22} & 0 & 0 & 0 & 0 \\ & & G_{11} & G_{12} & 0 & 0 \\ & & & G_{22} & 0 & 0 \\ & symm & & & B_1 & 0 \\ & & & & & 0 \end{matrix} \qquad (23)$$

where A_{11}, A_{12} and A_{22} are the conventional anisotropic elastic moduli and G_{11}, G_{12}, G_{22} and B_1 are the new Cosserat moduli which can be expressed as:

$$A_{11} = \frac{E}{1-\nu^2 - \dfrac{\nu^2(1+\nu)^2}{1-\nu^2+\dfrac{E}{hk_n}}}, \quad A_{22} = \frac{1}{\dfrac{1-\nu-2\nu^2}{E(1-\nu)}+\dfrac{1}{hk_n}}, \quad A_{12} = \frac{\nu}{1-\nu}A_{22} \qquad (24)$$

$$\frac{1}{G_{11}} = \frac{1}{G} + \frac{1}{hk_s}, \quad G_{11} = G_{12} = G_{21}, \quad G_{22} = G_{11} + G \qquad (25)$$

and $$B_1 = \frac{Eh^2}{12(1-\nu^2)}\frac{G - G_{11}}{G + G_{11}} \qquad (26)$$

where E is the Young's modulus, ν is the Poisson's ratio, h is the thickness and G is the shear modulus of the intact layer.

3. Numerical analysis

a) Numerical verification

The large deformation model has been implemented into the finite element code AFENA [15]. The finite element formulation is described in detail in Adhikary et. al [16]. For the verification of the model, the critical self-weight for a package of vertical layers was computed and compared with the analytical solution. Here, it was assumed that all the layers in the package buckle in the same manner.

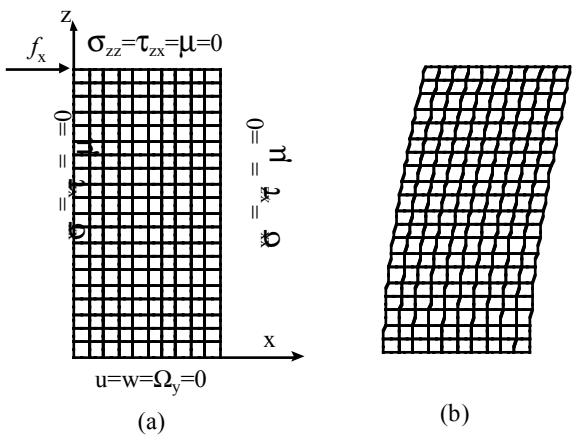

Figure 2. (a) Finite element mesh and the boundary conditions, (b) Deformed mesh

Figure 2a presents the finite element mesh and the boundary conditions adopted in this study. The problem region was discretised into 200 8-noded isoparametric quadrilaterals. The height (H) of the package composed of fifteen 1 m thick (h) layers was 30 m, the Young's modulus (E) was assumed to be unity and the Poisson's ratio (ν) was taken to be 0.16. The layer interface (joints) were assumed to possess zero shear stiffness and a normal stiffness $k_n h >> E$. A small perturbation (i.e. a small horizontal load, f_x) was applied at the top corner of the model.

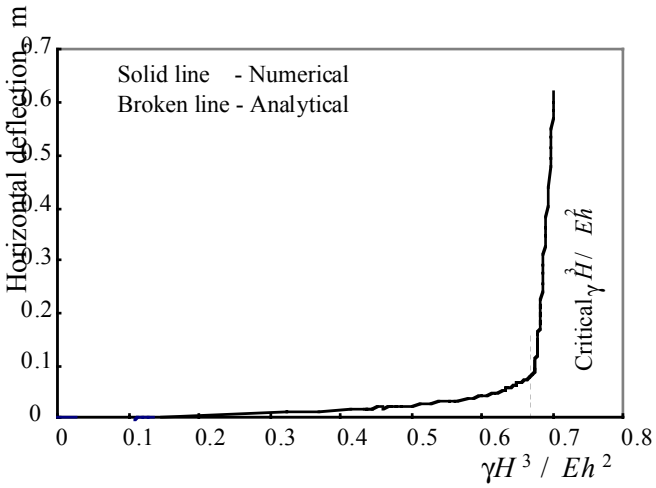

Figure 3. Load deflection plot for the case of a package of vertical layers

The problem was solved incrementally by increasing the self-weight (γ) of the layers in equal steps of 10^{-6} kN/m^3. Equilibrium iterations were conducted within each increment. In this study, the Newton-Raphson iteration scheme was adopted, where the displacement convergence tolerance [17] is set at 10^{-4}. Figure 2b presents the deformed mesh as the applied load approached the critical value.

Figure 3 presents the load-deflection curve obtained from the numerical computation. The analytical result, shown in this plot by a dashed line, was computed using the following expressions (Timoshenko, [18]):

$$\frac{\gamma H^3}{Eh^2} = 0.6575\left(1-\nu^2\right)^{-1} \tag{27}$$

It can clearly be seen that the computed critical load is in agreement with the theoretical solution (Eq. 27).

b) Flexural buckling of slopes

The numerical code is further used to analyse a buckling problem in a foliated rock mass. The rock layers are assumed to be 1 m thick and to possess the same elastic parameters as adopted in the previous example. A typical finite element mesh adopted in this analysis is shown in Figure 4. It consists of 410 8-noded isoparametric quadrilaterals. This finite element mesh configuration is chosen on the basis of a preliminary study of the convergence of the solution with mesh refinement. For this purpose, a slope angle of 80° is chosen and the problem region is discretised into 20, 31, 52, 139, 200, 252, 410, 620 and 810 8-noded isoparametric quadrilaterals and the critical loading parameter is computed in succession. The rock layers were assumed to dip parallelly to the slope face at an angle of 80°. Figure 5 presents a plot showing the convergence of the solution with mesh refinement. It can be seen that the convergence becomes much slower once the element number exceeds 400 mark. The computed critical loading parameter with 410 finite elements differ only marginally from that obtained with 810 finite elements. Thus, the rest of the calculations to follow are conducted by adopting similar finite element meshes as shown in Figure 4.

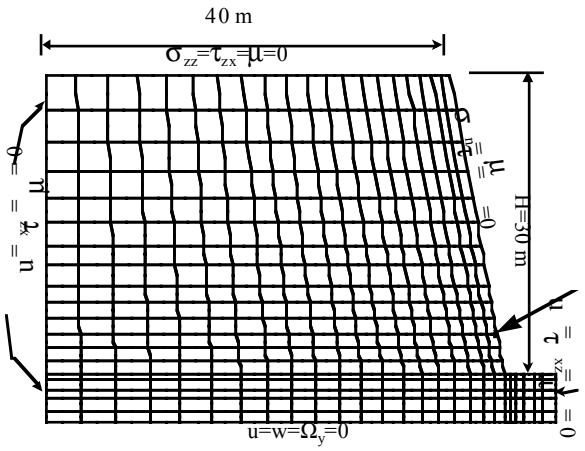

Figure 4. Finite element mesh and the boundary conditions used in the buckling analysis

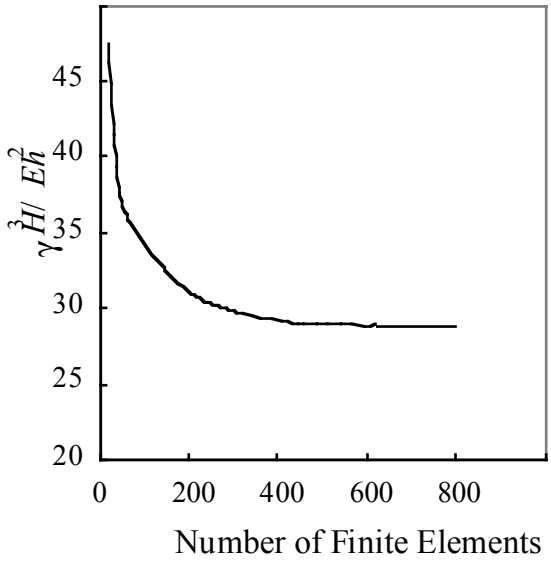

Figure 5. Convergence of solution with mesh refinement

Figure 6a presents the horizontal displacements of the node shown by an arrow in Figure 4 for the case of a 80° slope with zero joint friction. Results of both large deformation and small deformation analyses are shown in the figure. It can be seen that the small deformation model significantly under-estimates the deformation. However, the effect of large deformation becomes important only at higher load levels. The discrepancies between two model results are marginal at the load levels lower than about 50% of the critical buckling load.

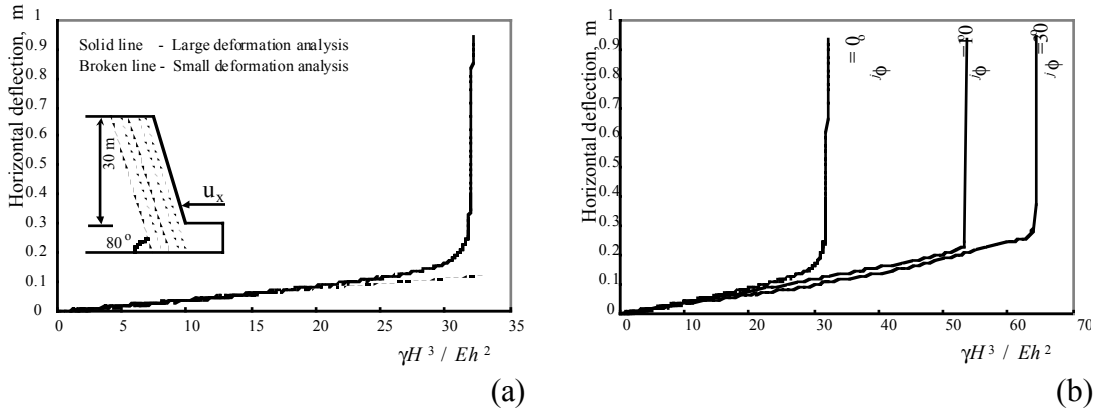

Figure 6. Load deflection curve for the case of buckling slope

Further calculations were conducted for joint friction angles of 10° and 30° and the obtained results are presented in Figure 6b. The results clearly show how a higher joint friction tends to increase the effective strength of the layered medium as a whole resulting in a higher buckling load.

In order to study the effects of slope angle on the buckling parameter, a number of calculations were performed for joint friction angles of 0°, 10°, 20°, 30° and slope angles of 90°, 89°, 88°, 85°, 80°, 75°, 70°, 65° and 60°. Figure 7 presents deformed meshes for the case of slope angles of 90°, 88°, 80° and 70°. From this figure, it can be seen that the effective length of the rock layer that undergoes buckling varies with the slope angles. The buckling mode for the case of the 90 slope agrees well with that of a single beam clamped at one end. However, it can be seen that the buckling mode changes drastically for non-vertical slopes. The effective length of the buckling layer is found to change drastically as the slope angle is decreased from 90° to 88° and so on. However, the change in effective length of the rock layer remains minimal once the slope angle becomes gentler.

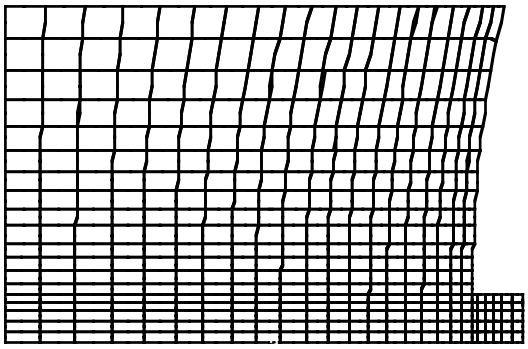

(a) Slope angle = 90°

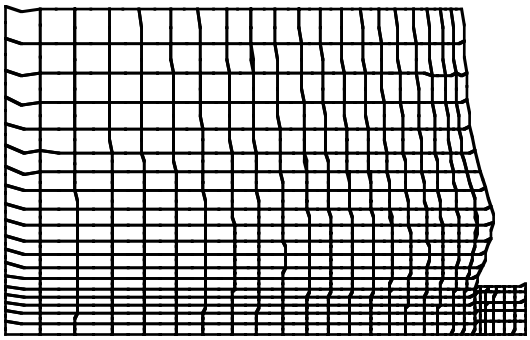

(a) Slope angle = 88°

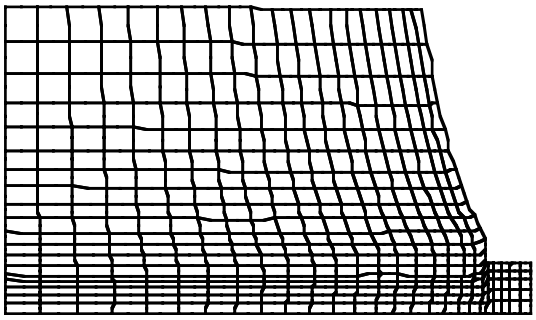

(a) Slope angle = 80°

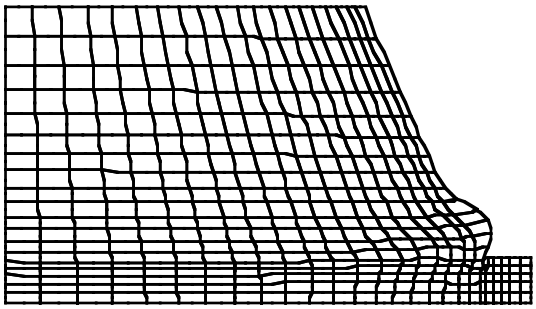

(a) Slope angle = 70°

Figure 7. Deformed meshes as the applied load approached the critical value

Table 1. Comparison of the Cosserat model and Cavers [1] model results

	Cosserat model results				Cavers (1981) model result			
α \ ϕ_j	0	10	20	30	0	10	20	30
80	26.99	47.98	55.98	60.98	4.45	4.59	4.75	4.95
85	23.99	35.99	45.98	51.99	4.40	4.47	4.54	4.63
90	0.55	0.67	0.72	0.77	4.38	4.38	4.38	4.38

Table 1 provides a comparison of critical loading factors for the 90°, 85° and 80° slopes as obtained by using Cavers [1] model (i.e. Eq. 1) and numerically using the Cosserat model. It can be seen clearly that the Cavers' model greatly overestimates the

critical loading factor for a vertical slope and substantially underestimates it for sub-vertical slopes.

On the basis of the numerical calculations conducted in this study, a chart suitable for the design of slopes in foliated rock masses is developed as presented in Figure 8. Four different plots are produced for the cases of 0°, 10°, 20° and 30° joint friction values. Since no consideration to the possibility of existence of cross joints and pore water is given in the present study, it is envisaged that this chart will provide an upper limit for a dry slope. In the presence of cross joins in the layers, the rock layer elastic modulus E used in the chart must be evaluated carefully by a proper consideration of the compliance of the cross-joints in the direction of layering. The computed effective elastic modulus of the rock layer may further be adjusted by an appropriate factor (so called the factor of safety) reflecting the margin of uncertainty involved in determining the effective elastic modulus.

Due to uncertainties involved in determining the rock mass parameters and also the exclusions of pore water and cross-joints made in the model formulation, it is recommended that the plot for joint friction angle of 0° (or possibly that for 10°) produced in Figure 8 be used for design purposes yielding a rather conservative slope design. For a 80° slope, the use of 0° (or 10°) plot will yield about 20 percent (or 6 percent) underestimation in critical slope heights in comparison to that computed using the plot for joint friction of 20°.

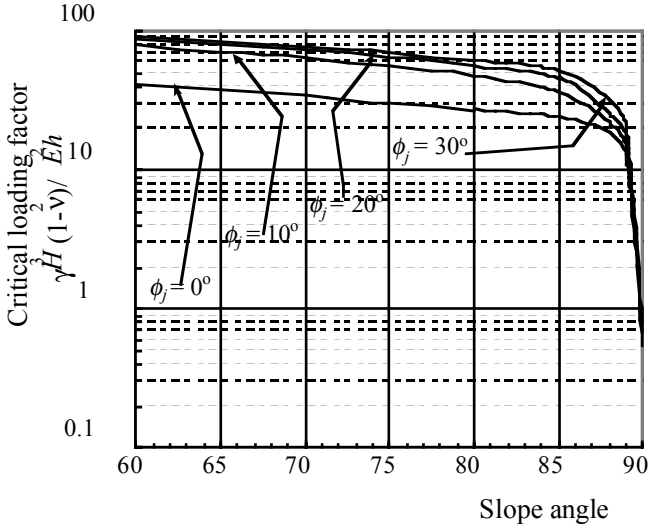

Figure 8. A design chart for foliated rock slopes against flexural buckling failures for the case of joint friction angles of 0°, 10°, 20° and 30°.

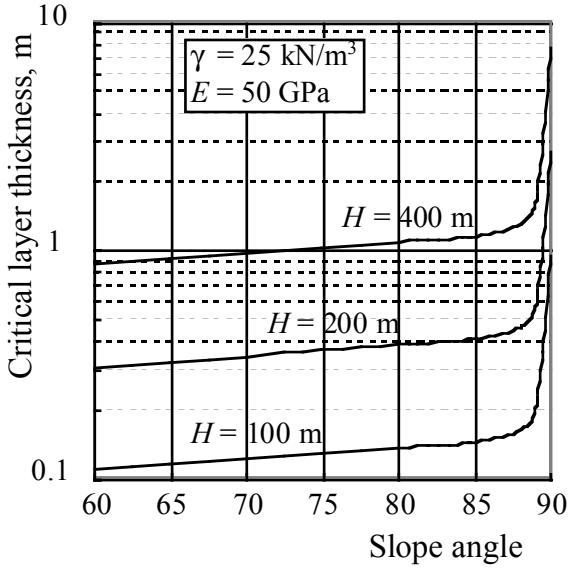

Figure 9. Critical layer thickness versus slope angle for slope heights of 100 m, 200 m and 400 m.

Figure 9 presents plots for critical layer thickness computed for a typical value of E=50 GPa, γ = 25 kN/m^3, slope heights of 100 m, 200m and 300m, and a zero joint friction angle. It can be seen that the buckling failure may be a possibility for a slope

angle of 80° for a slope height of 200 meters or more as long as the rock layer thickness (i.e. joint spacing) is less than 40 cm.

However, it is worthwhile to note here that the critical loading factors for sub-vertical slopes being relatively much higher in comparison to that for a vertical slope, it is imperative that a careful consideration must also be given for a possibility of other types of slope failures. A simple calculation can be conducted in the following manner to examine whether shear failure of the rock masses may precede any buckling failure. A conservative estimation of stable height of a slope can be computed as:

$$H_{shear} = \frac{\sigma_c}{\gamma} \tag{28}$$

where, H_{shear} is the critical height for the shear failure to occur, σ_c is the uniaxial compressive strength and γ is the unit weight of the intact rock layer respectively. This height H_{shear} must be greater than the height H_b (the critical height for buckling) for the possibility of any buckling type of failure to occur. The critical height H_b can be computed as follows:

$$H_b = \left(\frac{AEh^2}{\gamma}\right)^{1/3} \tag{29}$$

where, A is the critical loading factor that can be obtained from the design chart (Figure 8) for any particular slope angle. A combination of Eqs. (28) and (29) will yield the following inequalities necessary for any buckling failure to precede shear failure:

$$\left(\frac{AEh^2}{\gamma}\right)^{1/3} < \left(\frac{\sigma_c}{\gamma}\right) \tag{30}$$

The expression (30) can be arranged to obtain the following expression of a limiting layer thickness such that any layer thickness below this limiting value will produce a buckling type of failure for a particular slope if the critical slope height is attained.

$$h^2 < \frac{1}{A}\left(\frac{\sigma_c}{\gamma}\right)^2 \left(\frac{\sigma_c}{E}\right) \tag{31}$$

Figure 10 presents a plot for the limiting layer thickness for different slope angles for the case of σ_c/γ=500 and σ_c/E =0.001. In this example the critical loading factor A is obtained from Figure 8 for the case of zero joint friction. It can be clearly seen that, in the considered example, buckling failure may still be a possibility even for a 60° slope as long as the layer thickness remains less than 2.44 m.

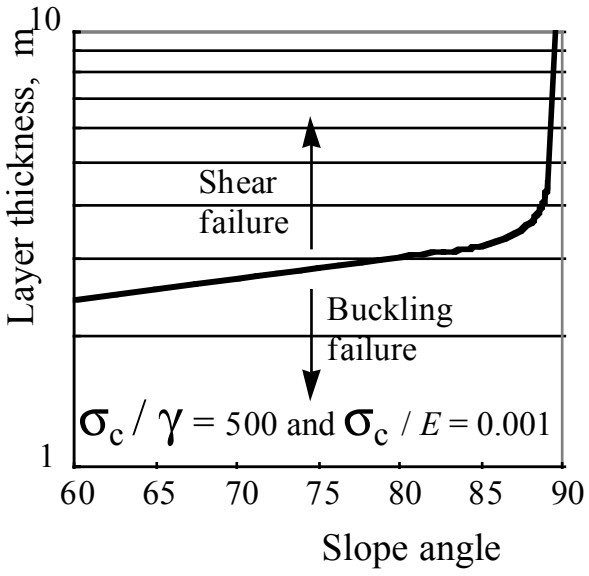

Figure 10. Plots of the limiting layer thickness where buckling can precede shear failure for the case of σ_c/E = 0.001

4. Conclusions

In this study, a large deformation model of foliated rock masses with elastic layers of equal mechanical properties and equal thickness has been devised on the basis of the Cosserat continuum theory and implemented into a finite element code. The layer interfaces (joints) are assumed to be rigid-perfectly plastic and are allowed to open in tension and yield in shear. It is found that the model can accurately predict the buckling load for a package of layers subjected to gravity loading. The Cosserat Finite element model is then subsequently used for computing the critical (buckling) loading factors for slopes excavated in a foliated rock mass. The computed critical loading factors are compared with those obtained using Cavers [1] model. It is found that the Cavers [1] model substantially overestimates the critical heights for vertical slopes and underestimates the same for sub-vertical slopes.

On the basis of this calculations, a design chart suitable for assessing the stability of foliated rock slopes against flexural buckling is presented. The design chart is envisaged to provide an upper limit for the critical loading factor for a dry slope as no considerations to the existence of pore water as well as cross-jointing is given in the present study. In the light of uncertainties involved in determining the rock mass parameters and the fact that the effect of pore water and cross-joints are ignored in the model formulation, it is recommended that the plot for joint friction angle of 0° (or possibly that for 10°) produced in Figure 8 be used for design purposes. For a 80° slope, the use of 0° (or 10°) plot will yield about 22% (or 6%) underestimation in critical slope heights in comparison to that computed using the plot for joint friction of 20°.

5 Acknowledgments

The authors are grateful to Prof. J.P. Carter of the University of Sydney for his permission to use the finite element program AFENA in this study. This work was supported by an Australian Research Council Large Grant (1996-1998); Grant No: A89600077.

6 References

1. Cavers, D.S., 1981. Simple methods to analyze buckling of rock slopes, *Rock Mech. Rock Engg*., vol. **14,** pp. 87-104.
2. Adhikary D.P., Dyskin, A.V. and Jewell, R.J., 1996. Numerical modelling of the flexural deformation of foliated rock slopes, *Int. J. Rock Mech. Min. Sci. And Geomech. Abstr.*, 33 (6), pp. 595-606.
3. Adhikary, D.P., Dyskin, A.V., Jewell, R.J. and Stewart, D.P., 1997. A study of the mechanism of flexural toppling failure of rock slopes, *Rock Mech. Rock Engg*., vol. **30**, No.2, pp. 75-94.
4. Adhikary, D.P. and Dyskin, A.V., 1998. Modelling of progressive and instantaneous failures of slopes in foliated rock masses, , *Int. J. Rock Mech. Min. Sci. And Geomech. Abstr*, submitted.
5. Kutter, H.K., 1974. Mechanism of slope failure other than pure sliding. Rock Mechanics, Int. Centre for Mechanical Sciences, Courses and Lectures No. 165, L.Muller (Ed), Springer, New York.
6. Corbyn, J.A., 1978. Stress distribution in laminar rock during sliding failure, *Int. J. Rock Mech. Min. Sci. And Geomech. Abstr.*, 15, pp. 113-119.
7. Hoek, E. and Bray, J.W., 1981. *Rock Slope Engineering*, Institution of Mining and Metallurgy, E & FN Spon, New York, pages 358.
8. Nilsen, B., 1987. Flexural buckling of hard rock - a potential failure mode in high rock slopes. *6th Int. Congr. On Rock mechanics*, Montreal, pp. 457-461
9. Froldi, P. And Lunardi, P., 1995. Buckling failure phenomena and their analysis, *Mechanics of Jointed and Faulted Rock*, Rossmanith (Ed.), pp.595-604.
10. Cosserat, E and Cosserat, F., 1909.*Theorie des corps deformables*, Hermann, Paris.

11. Mühlhaus, H.-B., 1993. Continuum models for layered and blocky rock, *Comprehensive Rock Eng*., Invited Chapter for Vol. **II**: Analysis and Design Methods, Pergamon Press, pp. 209-230.

12. Zvolinskii, N.V. and Shkhinek, K.N., 1984. Continual model of laminar elastic medium', *Mechanics of Solids*, **19** (1), pp. 1-9.

13. Adhikary, D.P. and Dyskin, A.V., 1997. A Cosserat continuum medium for layered media', *Computers and Geotechnics*, **20** (**1**), pp. 15-45.

14. Mühlhaus, H.-B., 1995. A relative gradient model for laminated materials, *Continuum Models for Materials with Micro-Structure*, H.-B. Mühlhaus (ed), Chap. 13.

15. Carter, J.P.and Balaam, N.G., 1995. *AFENA Users' Manual*. Centre for Geotechnical Research, University of Sydney, Australia, Version 5.

16. Adhikary, D.P., Mühlhaus, H.-B and Dyskin, A.V., 1998. Modelling the large deformations in stratified media - the Cosserat continuum approach, *Mechanics of Cohesive-Frictional Materials*, in print.

17. Bathe, K., 1982. *Finite Element Procedures in Engineering Analysis*, Prentice-Hall, Inc., New Jersey, 735 Pages.

18. Timoshenko, S., 1956. *Strength of materials*, Part **II**, pages 572.